THE JOURNAL OF PHYSICAL CHEMISTRY C

ARTICLE

pubs.acs.org/JPCC

Subwavelength Antireflective Si Nanostructures Fabricated by Using the Self-Assembled Silver Metal-Nanomask

Yuan-Ming Chang,*,† Jiann Shieh,‡ and Jenh-Yih Juang*,†

†Department of Electrophysics, National Chiao Tung University, Hsinchu 300, Taiwan

‡Department of Materials Science and Engineering, National United University, Miaoli 360, Taiwan

ABSTRACT: We report a lithography-free approach for fabricating silicon nanopillars (Si-NPs) and biomimetics porous silicon (P-Si) with excellent antireflective properties. The self-assembled silver nanostructures (nanoislands and disordered nanogrids) were formed via the Volmer−Weber (island growth) mode during the deposition process, which, in turn, serve as a metal-nanomask for the subsequent dry etching process carried out for fabricating the Si-NPs and P-Si on Si substrates. Reflectivity of about 0.65% was obtained over the spectral region ranging from deep-ultraviolet to infrared light (300−1000 nm). The remarkable antireflective characteristics obtained are attributed to the drastic decrease of effective index of refraction and the enhanced matching effect between air and substrate resulting from the Si nanostructures and suggesting an interesting alternative route for producing nanostructures that might be useful for photovoltaic applications.

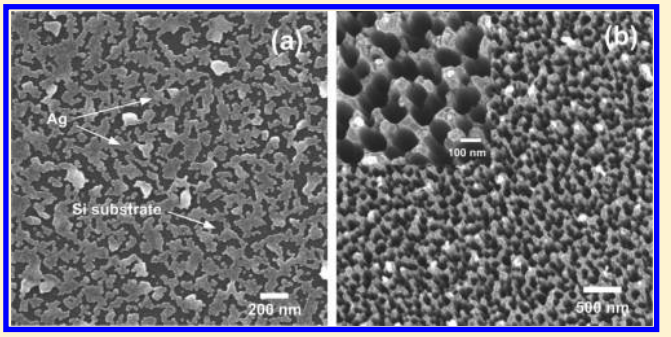

1. INTRODUCTION

Silicon nanostructures, including silicon nanocones, silicon nanopillars (Si-NPs), and porous silicon (P-Si), have attracted tremendous research interest over the past decade owing to their potential in a wide variety of applications, such as biosensors,[1−3] photodetectors,[4,5] photovoltaic devices,[6,7] and photonics.[8] Among them, the application to photovoltaic cells for enhancing the efficiency of solar energy harvesting has emerged as a top issue. One of the major obstacles that seriously decrease the conversion efficiency of photovoltaic devices is the loss of light due to reflection. For that matter, fabricating structures with greatly enhanced antireflective properties on surfaces of the solar cells has become a hotly pursued subject for improving the photovoltaic conversion efficiency.[9−11] In most of the demonstrated structures the reduction of reflection loss has been attributed to either the distortion of the radiation wavefront to achieve light trapping by total internal reflection inside the surfaces or to the tapered index of refraction resulting from the subwavelength nanostructures obtained. Moreover, the short collection length for excited carriers enabled by incorporating the Si nanostructures into solar cells also might be beneficial in solar energy harvesting.

Previously, various methods,[12−15] ranging from photolithography etching to spin coating, have been used to prepare the subwavelength structures. The obtained nanostructures satisfactorily demonstrated an average reflectance of 2−10% within the wavelength range of 300−900 nm. The applicability of these techniques, however, either is specific to certain wavelengths or is hindered by the stability problems associated with the undesired adhesion issues between nanostructures and substrate. To resolve the above-mentioned issues, very recently much improved antireflective performance with Si-nanotips exceeding micrometer length has been obtained by a self-masking electron cyclotron resonance etching process.[10] In this study, we report an alternative method of using the self-assembled silver nanostructures as the metallic-nanomask to fabricate the Si-NPs and biomimetics (sponge-like) structures of P-Si. Since the silver nanoislands and disordered nanogrids were formed through Volmer−Weber growth mode during sputtering and the direct dry etching was subsequently performed, the Si-NPs and P-Si nanostructures were obtained very effectively: usually it took less than 10 min for obtaining 1 μm-long Si-NPs. The simplicity of the current fabrication method thus is advantageous in several respects. First, the manufacturing process is very effective because it took only 10−20 s to obtain the self-assembled silver-nanomask by sputtering. Moreover, the lithography-free anisotropic dry etching can reduce the fabrication cost significantly. Finally, the presented Si-NPs and P-Si has an average reflectance as low as 0.65% in the broadband wavelength range from 300 to 1000 nm (deep ultraviolet (DUV) to infrared ray (IR)), respectively, which by far is superior to that obtained in most antireflective Si-nanostructures.

2. EXPERIMENTAL SECTION

The Ag nanoislands grown on Si substrates were obtained by rf-sputtering from an Ag target (Eastern Sharp EPS01) for

Received: March 1, 2011
Revised: April 8, 2011
Published: April 18, 2011

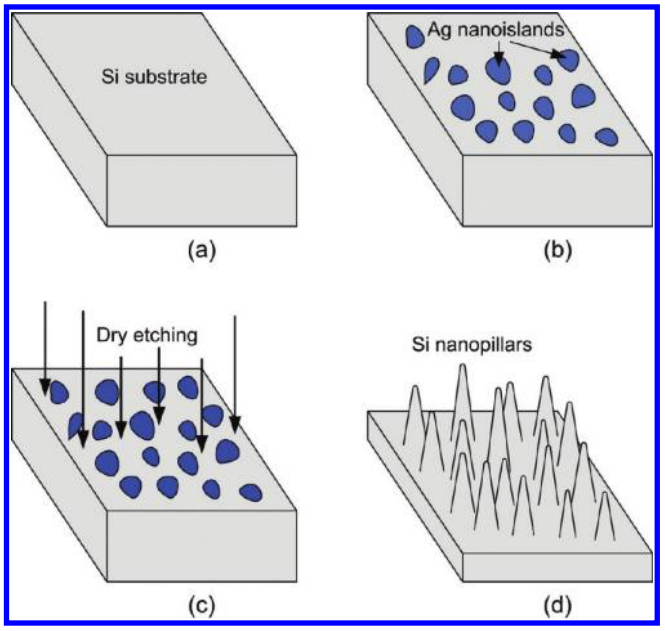

Figure 1. Steps in the fabrication of Si-NPs: (a) Si substrate with p-type (100), (b) Ag nanoislands are formed from sputtering, (c) dry etching by plasma, and (d) finally the Si-NPs are fabricated.

10−20 s with an input power of 150 W in 25 sccm argon gas atmosphere. As illustrated schematically in Figure 1b, due to the short sputtering time practiced, the resulting size distribution of the obtained Ag nanoislands is rather uneven. The Si-NPs array was obtained by subsequent dry etching performed in a metal etcher system (Canon ILD 4100). Prior to etching, the chamber was evacuated to a base pressure of 3×10^{-5} Torr while the system temperature was kept at 60 °C. After loading the prepared Ag nanoislands covered Si substrate, Cl_2 gas of 90 sccm and N_2 gas of 10 sccm were introduced. The system was operated with a fixed input power of 1900 W maintained and the etching time was varied from 1 to 20 min. This process is also depicted schematically in Figure 1c. During the dry etching process, the reactive ions were accelerated and passed the sheath region to produce the ion bombardment effect that, in turn, etches the Si substrates anisotropically to form the Si-NPs, as illustrated schematically in Figure 1d. The P-Si structures were obtained similarly except that in this case the rf-sputtering time of Ag was prolonged to 20 s and the obtained Ag nanoislands started to coalescence and formed irregularly connected grains on the Si substrate. The reflectivity of both of the Si-NPs and P-Si's was measured with a spectrophotometer (Jasco V-670) with unpolarized light of wavelengths ranging from 300 to 1000 nm. To obtain precise information on the optical properties of the Si-NPs and P-Si's, an integrating sphere was used in the spectrophotometer to determine the total reflectance.[16]

3. RESULTS AND DISCUSSION

Figure 2a exhibits the SEM image showing the typical morphology and distribution of the Ag nanoislands obtained with a sputtering time of 10 s. The density of the Ag nanoislands is estimated to be around 4.5×10^9 cm^{-2}. The area density of the Ag nanoislands is about 2 orders of magnitude smaller than that reported by Lin et al.[17] where the self-aggregated Ni-nanodots with an area density of 5×10^{11} cm^{-2} were obtained by carrying out the rapid thermal annealing process on a 50-nm-thick e-beam evaporated Ni layer at 850 °C for 22 s. Furthermore, it is evident from the SEM image that, in addition to the isolated islands with smaller sizes, there appears to be islands resulting from coalescence of two or more islands already in this short sputtering time. Both of these characteristics are believed to result from the film growth mechanism inherent to the current system and can be understood as follows. Since the surface energies for silver and SiO_2 are about 923 ergs/cm^2 and 200−260 ergs/cm^2, respectively,[18] one expects that the deposited Ag layer would follow the Volmer−Weber growth mode and grow into island-like morphology during the processes of sputtering. The formation of the growing islands thus is by the nucleation and growth mechanism and is prevailed predominantly by surface diffusion of the impingement of condensate monomers, rather than the thermal-induced dewetting and subsequent agglomeration of an existing thin layer.[13−15] It has been reported that, for Ag or Au condensed on MoS_2 substrate kept at 400 °C, the density of the initial nuclei was about 5×10^{10} cm^{-2} with a typical diffusion distance of 50 nm and the coalescence of these nuclei can occur in less than 0.1 s.[19] It is, thus, quite reasonable to observe a much lower area island density and apparent island coalescence in the present case even within a "short" sputtering time of 10 s.

Figure 2b displays the Si-NPs obtained from Si substrate partially covered with the Ag nanoislands shown in Figure 2a after performing the dry etching process for 1 min. The Si-NPs obtained under this condition have an average height of 50 to 150 nm and an aspect ratio of ∼1 with the masking Ag nanoislands remaining nearly intact at the tip of the Si-NPs. Obviously, the Ag nanoislands acted as an effective metal-nanomask during the early stage of dry etching performed on the Si substrate. The formation of Si-NPs thus was a natural consequence of the protection from Ag nanoislands, which protect the areas underneath from ion bombardment during the dry etching process while significant anisotropic etching prevailed on the exposed areas of the Si substrate.

By increasing the etching time, the height of the Si-NPs was found to grow continuously while the coverage of the masking Ag nanoislands was diminishing at the same time. We found that at an etching time of about 10 min the Ag nanoislands appeared to vanish completely. The Si-NPs obtained with 10 min etching time, as displayed in Figure 2c, are aligned vertically along the [001] crystallographic orientation with the average height and width being about 1 μm and 100−200 nm, respectively. The latter and the spacing between the Si-NPs are, in fact, consistent with the size of the Ag nanoislands (Figure 2a), indicating the effectiveness of using them as etching masks. It turned out that in the present case 10 min etching has resulted in an optimal compromise between the etching rate selectivity and mask protection effectiveness for Si substrates. Indeed, as shown in Figure 2d for the case of increasing the etching time to 20 min, further etching without the masking protection of Ag nanoislands evidently leads to complete destruction of the Si-NPs.

Another antireflective Si nanostructure of interest is the biomimetics (sponge-like) structures of P-Si, which turns out can also be easily fabricated with the current process. Inspired by the above-mentioned growth mechanism underlying the growth and coalescence of the Ag nanoislands formed in situ during the sputtering process, we have intentionally prolonged the sputtering time to 20 s. Figure 3a shows the morphology of the resulting Ag film obtained after the prolonged sputtering process.

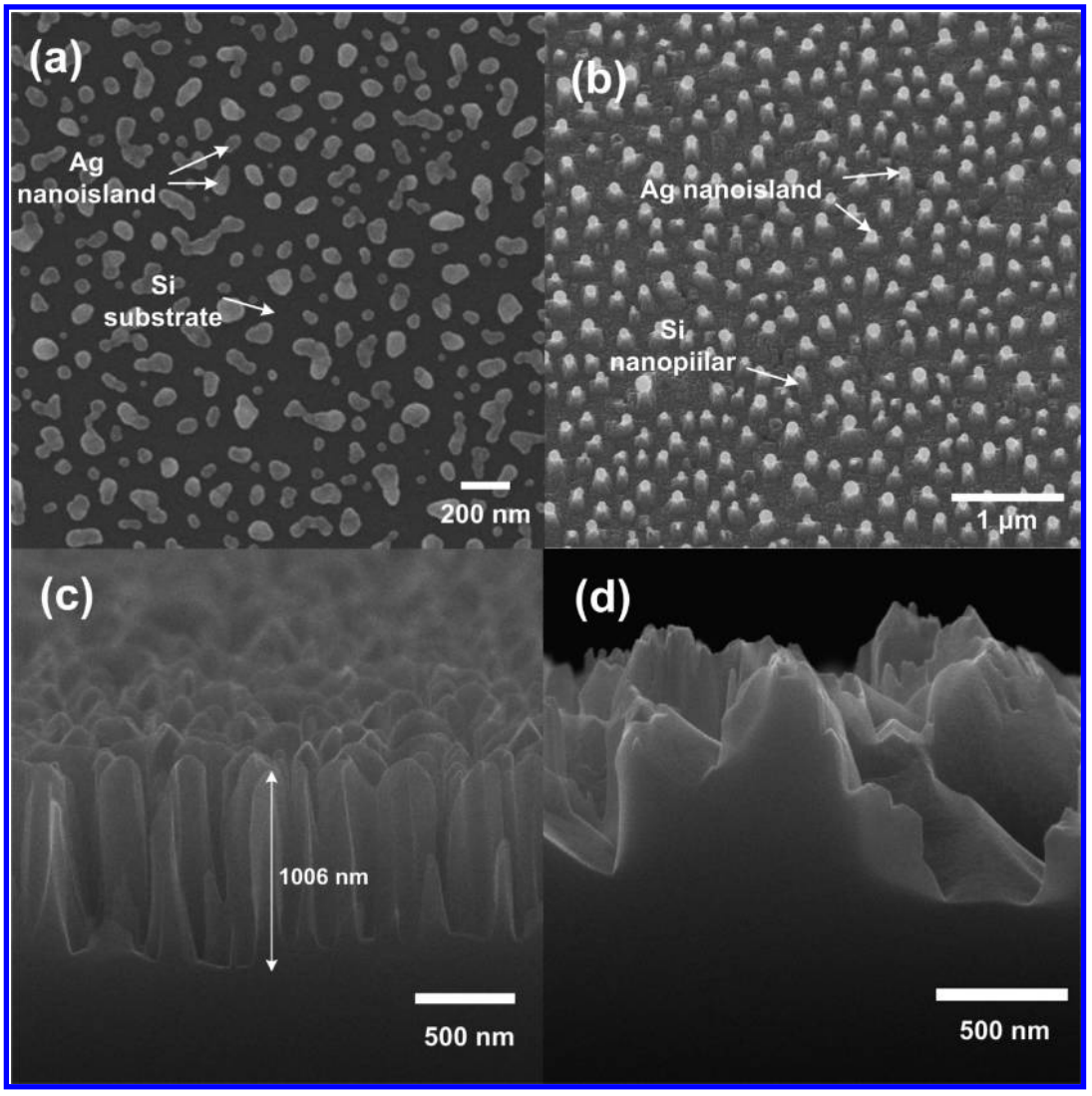

Figure 2. (a) The SEM images of Ag nanoislands evenly distributed on Si substrate; (b) the SEM image of Si-NPs that have been processed by dry etching for 1 min; (c) the SEM image of Si-NPs that are fabricated by dry etching for 10 min; and (d) the Si-NPs have been annihilated after a dry etching time of 20 min.

Comparing to the result shown in Figure 2a, it is clear that such prolonged sputtering time was adequate to drive the deposited Ag film from the island coalescence stage into the island-networking growth stage. The morphology of the obtained Ag film, though appearing to be rather disordered, is ideal to serve as an etching mask for fabricating biomimetics P-Si. Figure 3b shows the resulting substrate structure after carrying out 10 min of dry etching on Si substrate covered by Ag film shown in Figure 3a. In this case, connecting the porous structure with approximately 1-μm-deep holes (see the inset of Figure 3b) is evidently obtained. However, unlike the results displayed in Figure 2, there appears to still be traces of Ag metal masks left on the surface of the obtained structure. This is not surprising because the thickness of the Ag layer is presumably much thicker than that of the one shown in Figure 2 due to the twice longer sputtering time practiced. In any case, we have demonstrated that the Ag nanoislands obtained in situ by short time sputtering can indeed serve as effective metal masks for fabricating structures such as Si-NPs and P-Si. Next we turn to discussing the optical properties of these structures.

The total reflectance spectra to be presented in the following, including the specularly reflected beam, were measured by an integrating sphere with the wavelength ranging from ultraviolet to near-infrared. Figure 4 displays the reflectance as a function of measuring wavelength, ranging from 300 to 1000 nm, for the as-polished Si substrate, Si-NPs obtained with various dry etching durations (namely for 1, 5, 10, and 20 min, respectively), as well as for the P-Si structure described above. From the curves displayed in Figure 4, it is evident that the polished Si substrate (solid aquares) exhibits the typical wavelength-dependent reflectance with the mean reflectance as high as 38% in the 500−1000 nm wavelength range. The reflectance is significantly suppressed even with the surface featuring Si-NPs with relatively low aspect ratio obtained by dry etching for 1 min (as shown in Figure 2b). However, due to the lack of sufficient height, the reflectance of these nanostructures remains at the level of about 11.9% over the spectrum range from 300 to 1000 nm. The short pillar structure also may be responsible for the increasing reflectance seen at longer wavelengths (λ > 700 nm), presumably due to the existence of residual Ag nanoislands at the tip of the

dx.doi.org/10.1021/jp201973y |J. Phys. Chem. C 2011, 115, 8983–8987

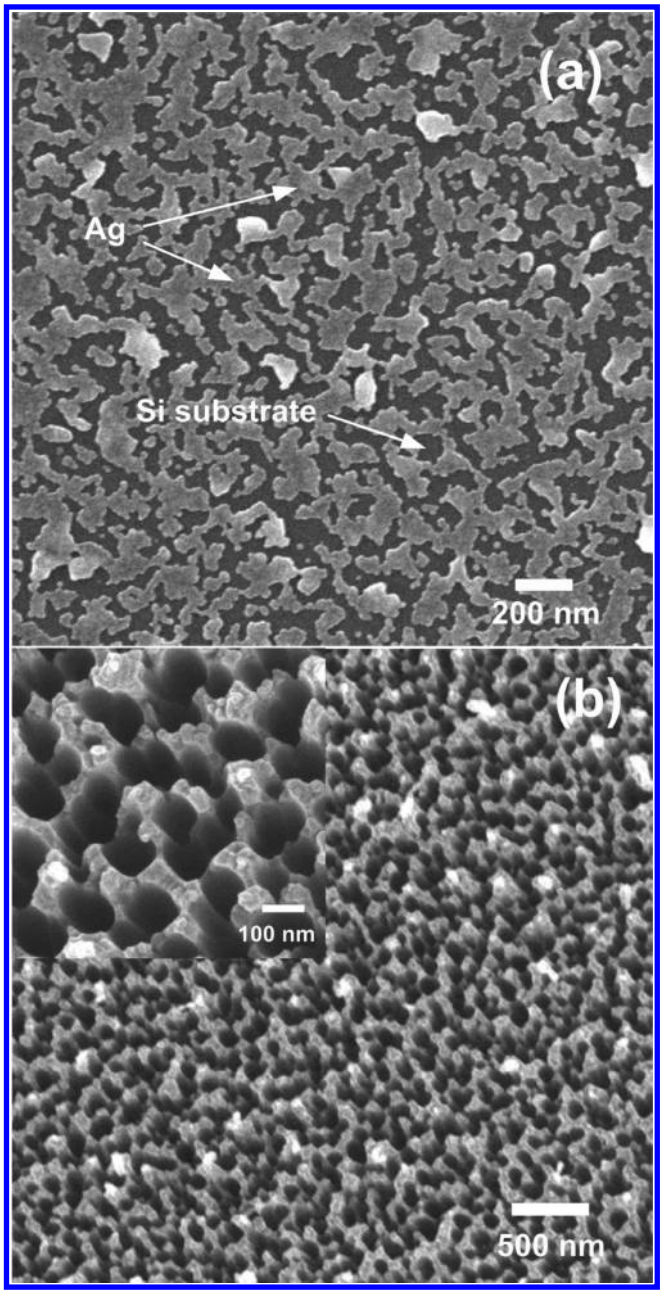

Figure 3. The SEM images of (a) Ag disordered nanogrids (sputtering time of 20 s) distributed on Si substrate and (b) P-Si. The inset is the high-magnification SEM image of P-Si.

Si-NPs as well as the inactive $\lambda/4$ antireflection effect. The situation is further improved by increasing the time duration of dry etching to 5 min. As is evident from the results, owing to the increased height of the obtained Si-NPs, the mean reflectance was further suppressed to 5.49%.

Perhaps the most significant result of the current study is that the average reflectance is suppressed to 0.65% over the entire spectral bandwidth ranging from 300 to 1000 nm when the substrate was processed with a dry etching duration of 10 min. This is about 1.5 orders of magnitude smaller than that of the polished Si. Obviously, the height of Si-NPs is playing a key role.[20,21] This can be understood as follows. An ideal antireflection coating should satisfy the following conditions: $n_c = (n_a n_s)^{1/2}$, where n_c, n_a, and n_s represent the refractive indices of the

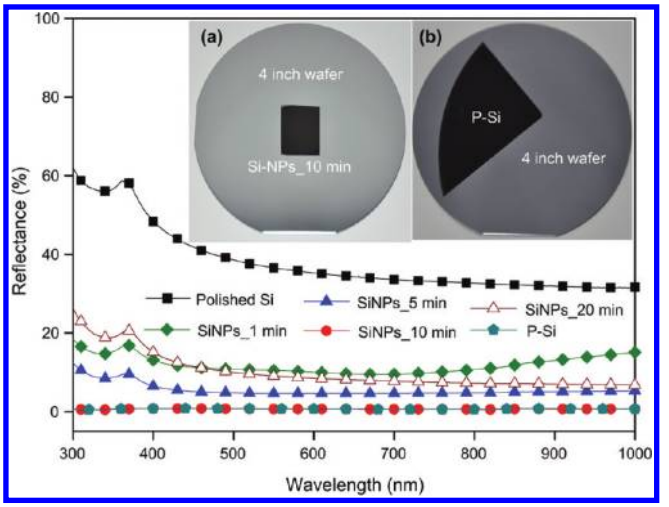

Figure 4. The reflectivity spectroscopy for polished Si, P-Si, and Si-NPs with dry etching times of 1, 5, 10, and 20 min. The inset shows the (a) P-Si and (b) Si-NPs with dry etching for 10 min taken with a digital camera.

coating material, air, and substrate, respectively. Moreover, reflection loss can be decreased at wavelengths near the quarter-wavelength optical thickness.[22] Thus, in order to suppress the reflection, n_c must be between 1.2 and 1.3.[23] However, the lowest refractive index of the applied materials is about 1.34.[24] Under this circumstance, one of the effective ways of decreasing the n_c value is to use appropriate structures to introduce air into the surfaces. Furthermore, when the incident light reaches the interface between two media, the reflection is determined by the difference in their refractive indices. Thus it would be even more effective to suppress the reflection if some sort of gradual refractive index gradient can be established.[21] In the present case, the one-dimensional Si-NPs (with height of 1 μm) not only drastically reduced the effective refractive index in the Si-NPs layer by introducing significant empty space and surface areas but also form a gradually decreasing refraction index gradient from substrate to air because of the spear-shape pillars. Both are believed to result in very low reflectance obtained by these micrometer-sized Si-NPs arrays. Additionally, since the spacing between the Si-NPs is mostly much smaller than the incident wavelength, the diffraction losses can also be avoided in the current Si-NPs structure.[25] On the other hand, when the Si-NPs were destroyed by prolonged etching (e.g., the surface morphology obtained after 20 min etching duration shown in Figure 2d), the remaining irregular surface alone cannot effectively suppress the reflection and the measured reflectance rising back to a level of 9.14% over the same spectral bandwidth measured.

Although the results presented above have demonstrated that Si-NPs can be fabricated and indeed exhibit excellent antireflective properties, it is noted that the pillar structure is also quite susceptible to subtle process parameters, such as the sputtering and the dry etching durations. To further take advantage of the Ag metal-nanomask for fabricating nanostructures with equally high-performance and scale-up viabilities, we have also extended the present concept to fabricate P-Si nanostructures, as briefly described in Figure 3. According to Figure 3b, the surface of the P-Si obtained by dry etching the Si substrate covered with connected Ag islands is highly porous. The sponge-like structure consists of a large surface area resulting from holes of 100 nm diameter and ridges protected by the Ag islands randomly

distributed on the resulting Si substrate (see the inset in Figure 3b). As is evident from Figure 4 (solid pentagons), the biomimetic P-Si sample exhibits essentially the same antireflective property as that of the 10 min dry etching Si-NPs (solid circles) with an average reflectance below 0.69%. Since both samples were subjected to the same etching time duration, we expect that both should have similar etching depth and hence similar effects in suppressing the reflection loss, namely by effectively reducing the value of the index of refraction and trapping the incident lights inside the structures. Finally, as illustrated in the insets of Figure 4, both optical pictures clearly contrast the dark appearances exhibited in the regions with Si-NPs (inset to panel a) and P−Si (inset to panel b) to the shinning appearance exhibited in original polished Si substrate. We note that the ease of fabricating the Si-NPs and P-Si structures and the excellent antireflective properties demonstrated in both structures with the present processes should have significant implications in potentially incorporating them into the photovoltaic applications.

4. CONCLUSIONS

In summary, we have demonstrated that by properly manipulating the time duration of Ag sputtering and the subsequent dry etching process, Si nanostructures (including Si-NPs array and biomimetics sponge-like structure) with reflectance as low as 0.65% can be easily obtained. Comparing to most of the techniques employed in obtaining similar structures, not only the antireflective performance is comparable to the best results reported, but also the current process is simple and, more importantly, lithography-free. The in situ formation of Ag nanoislands during the rf-sputtering process was found to follow the surface diffusion dominated three-dimensional nucleation and growth (the Volmer−Weber) mechanism. The island coalescence stage was observed to occur within 10 s of sputtering time and the subsequent island networking was nearly completed in 20 s. By using these self-assembled Ag nanostructures (islands and disordered island networks) as the metal-nanomasks, Si-NPs and P-Si were obtained by subsequent dry etching. The obtained Si-NPs and P-Si exhibit an average reflectance of 0.65% and 0.69% over the wavelength range between 300 and 1000 nm, respectively, which is about 1.5 orders of magnitude smaller than that of the polished Si. The present technique, with its simplicity and effectiveness, has evidently provided significant application potentials in a variety of fields, especially in biomimetics-based nanodevices and high-efficiency photovoltaic devices.

AUTHOR INFORMATION

Corresponding Author

*To whom correspondence should be addressed. E-mail: ymchang7@gmail.com (Y.-M.C.), jyjuang@g2.nctu.edu.tw (J.-Y.J.). Fax: +886-3-5725230. Phone: +886-3-5712121 ext. 56116.

ACKNOWLEDGMENT

This work was partially supported by the National Science Council of Taiwan, under Grant No. NSC 99-2811-M-009-057. J.Y.J. is supported in part by the National Science Council of Taiwan and the MOE-ATP program operated at NCTU. The authors would like to thank Prof. Hsi-Fu Shih (NCHU), Prof. Ching-Liang Dai (NCHU), and Jyun-Hao Wu for sputtering (NCHU), Prof. Hsin-Yi Lee (NSRRC and NCTU), Porf. Chih-Ming Lin (NHUE), Dr. Yu-Hwa Shih, Chih-Ming Wu, and Chih-Yen Shen for useful discussions, Hung-Min Lin for TEM, Yi-Ling Jian and Chiung-Chih Hsu for SEM, and Mei-Yi Liao for spectrophotometric technical supports in National Nano Device Laboratories.

REFERENCES

(1) Zhang, G.-J.; Zhang, G.; Chua, J. H.; Chee, R.-E.; Wong, E. H.; Agarwal, A.; Buddharaju, K. D.; Singh, N.; Gao, Z.; Balasubramanian, N. *Nano Lett.* **2008**, *8*, 1066.

(2) Li, Z.; Chen, Y.; Li, X.; Kamins, T. I.; Nauka, K.; Williams, R. S. *Nano Lett.* **2004**, *4*, 245.

(3) Lin, V. S.-Y.; Motesharei, K.; Dancil, K.-P. S.; Sailor, M. J.; Ghadiri, M. R. *Science* **1997**, *278*, 840.

(4) Lee, M.-K.; Chu, C.-H.; Wang, Y.-H. *Opt. Lett.* **2001**, *26*, 160.

(5) Zheng, J. P.; Jiao, K. L.; Shen, W. P.; Anderson, W. A.; Kwok, H. S. *Appl. Phys. Lett.* **1992**, *61*, 459.

(6) (a) Lipinski, M.; Panek, P.; Swiatek, Z.; Beltowska, E.; Ciach, R. *Sol. Energy Mater. Sol. Cells* **2002**, *72*, 271. (b) Yerokhov, V. Y.; Hezel, R.; Lipinski, M.; Ciach, R.; Nagel, H.; Mylyanych, A.; Panek, P. *Sol. Energy Mater. Sol. Cells* **2002**, *72*, 291.

(7) Aroutiounian, V. M.; Maroutyan, K. R.; Zatikyan, A. L.; Touryan, K. J. *Thin Solid Films* **2002**, *403*, 517.

(8) Parker, A. R.; Townley, H. E. *Nat. Nanotechnol.* **2007**, *2*, 347.

(9) Peng, K.; Xu, Y.; Wu, Y.; Yan, Y.; Lee, S.-T.; Zhu, J. *Small* **2005**, *1*, 1062.

(10) Huang, Y.-F.; Chattopadhyay, S.; Jen, Y.-J.; Peng, C.-Y.; Liu, T.-A.; Hsu, Y.-K.; Pan, C.-L.; Lo, H.-C.; Hsu, C.-H.; Chang, Y.-H.; Lee, C.-S.; Chen, K.-H.; Chen, L.-C. *Nat. Nanotechnol.* **2007**, *2*, 770.

(11) Li, X.; Li, J.; Chen, T.; Tay, B. K.; Wang, J.; Yu, H. *Nanoscale Res. Lett.* **2010**, *5*, 1721.

(12) Sun, C.-H.; Min, W.-L.; Lin, N. C.; Jianga, P.; Jiang, B. *Appl. Phys. Lett.* **2007**, *91*, 231105–1.

(13) Park, S.-J.; Lee, S.-W.; Lee, K.-J.; Lee, J.-H.; Kim, K.-D.; Jeong, J.-H.; Choi, J.-H. *Nanoscale Res. Lett.* **2010**, *5*, 1570.

(14) Lalanne, P.; Morris, G M. *Nanotechnology* **1997**, *8*, 53.

(15) Lee, Y.; Koh, K.; Na, H.; Kim, K.; Kang, J.-J.; Kim, J. *Nanoscale Res. Lett.* **2009**, *4*, 364.

(16) Chang, Y. M.; Dai, C. L.; Cheng, T. C.; Hsu, C. W. *Thin Solid Films* **2010**, *518*, 3782.

(17) Lin, G. R.; Chang, Y. C.; Liu, E. S.; Kuo, H. C.; Lin, H. S. *Appl. Phys. Lett.* **2007**, *90*, 181923–1.

(18) Bondi, A. *Chem. Rev.* **1953**, *52*, 417.

(19) Maissel, L. I.; Glang, R. *Handbook of Thin Film Technology*, McGraw-Hill: New York, 1970; Chapter 8.

(20) Shieh, J.; Lin, C. H.; Yang, M. C. *J. Phys. D: Appl. Phys.* **2007**, *40*, 2242.

(21) Zhu, J.; Yu, Z.; Burkhard, G. F.; Hsu, C. M.; Connor, S. T.; Xu, Y.; Wang, Q.; McGehee, M.; Fan, S.; Cui, Y. *Nano Lett.* **2009**, *9*, 279.

(22) Hiller, J.; Mendelsohn, J. D.; Rubner, M. F. *Nat. Mater.* **2002**, *1*, 59.

(23) Hattori, H. *Adv. Mater.* **2001**, *13*, 51.

(24) Cao, M.; Song, X.; Zhai, J.; Wang, J.; Wang, Y. *J. Phys. Chem. B* **2006**, *110*, 13072–13075.

(25) Clapham, P. B.; Hutley, M. C. *Nature* **1973**, *244*, 281.